COOLANT SOLUBILITY OF BURNABLE NEUTRON ABSORBING MATERIAL: A THERMODYNAMIC TREATMENT IN SUPPORT OF ADVANCED CANDU® REACTOR FUEL

A.S Blackier[1], E.C. Corcoran[1], M.H. Kaye[2] and W.T. Thompson[1]

[1] Royal Military College of Canada, Ontario, Canada
P.O. Box 17000, St. Forces, Kingston, Ont., Canada K7K 7B4

[2] *University of Ontario Institute of Technology*
Faculty of Energy Systems and Nuclear Science
2000 Simcoe Street North, Oshawa Ontario L1H 7K4

ABSTRACT

The Advanced CANDU® Reactor (ACR) employs a newly-designed fuel bundle that contains a Burnable Neutron Absorbing (BNA) material in the central position. The BNA is composed of elements with high neutron absorption cross sections (Gd and Dy) dissolved in zirconia. If a sheath failure were to occur, there is concern that the possible leaching of these elements into the coolant could cause a reactivity re-distribution. To address this concern, the solubility of Gd and Dy over a range of pH and temperatures has been examined in the context of the possible existence of hydroxyl complex ions. Estimated thermodynamic properties are proposed that provide the means to compute the low Dy and Gd concentrations in the reactor coolant in the event of a BNA cladding breach.

1. Introduction

The Advanced CANDU® Reactor[1] (ACR-1000) is planned to be the next generation in AECL electrical power reactor designs. The ACR-1000 incorporates the proven strengths of the existing CANDU® reactors while improving reactor safety and economics [1].

To reduce initial capital cost, the ACR-1000 will incorporate a more compact core design and a reduction in heavy water inventory by replacing the heavy water coolant with conventional light water. The substitution of light water for heavy water will decrease the total heavy water inventory (coolant and moderator) by approximately 50 percent in comparison to CANDU®-6 reactors [1].

The unique enabling technology of the ACR-1000 is the fuel bundle design. The ACR-1000 fuel bundle is based on the CANFLEX (43 element) design. The three outer rings of fuel elements

[1] 1000 MW_e output

(42 elements) contain low enriched uranium (LEU) dioxide fuel (approximately 2 at% ^{235}U), a marked departure from the CANDU® fuel design of the last forty years. The central element contains a Burnable Neutron Absorber (BNA) material. A depiction of the ACR-1000 fuel bundle (end view) is shown in Figure 1.

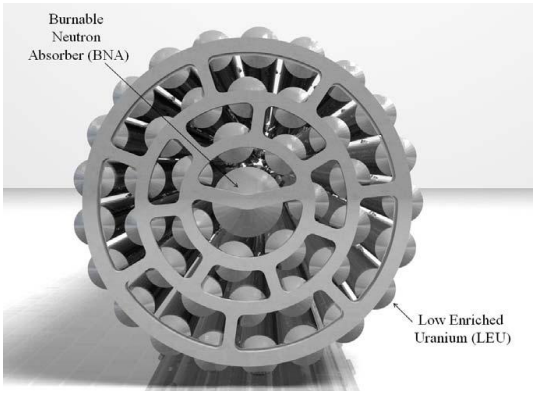

Figure 1. Cross sectional view of ACR-1000 CANFLEX fuel bundle [1,12].

The BNA contributes to a negative void coefficient by decreasing the thermal neutron flux at the centre of the fuel bundle in the event of coolant voiding [2,3]. The BNA is a sintered oxide material of dysprosia ($Dy_2O_{3\,s}$) and gadolinia ($Gd_2O_{3\,s}$) in a matrix of cubic yttria ($Y_2O_{3\,s}$) and stabilized zirconia ($ZrO_{2\,s}$). The active elements with respect to neutron absorption are dysprosium (*Dy*) and gadolinium (*Gd*). Both elements have a large neutron absorption cross section. In absorbing neutrons, dysprosium and gadolinium transmute to holmium (Ho) and terbium (Tb), respectively [4]. Since Ho and Tb have relatively low neutron absorption cross sections, the ability of the BNA material to consume neutrons decreases slowly as irradiation progresses, hence the name "Burnable" Neutron Absorber. The buildup in fission products in the active fuel elements compensates.

If the protective sheathing of the central BNA element were to fail while in operation, the BNA material would come into contact with the coolant. Depending on the solubility of the BNA for the conditions of pH involved, dysprosium and gadolinium could dissolve to some extent in the coolant. The large neutron capture cross sections of the dysprosium and gadolinium circulating in the reactor core have the potential to disrupt the neutron economy of the entire reactor. Therefore, the solubility of BNA under CANDU® operational conditions must be well understood. Further, this understanding must be expressed in such a way that the extent of BNA solubility can be incorporated into extremely broad-based fuel performance models. In particular, the BNA solubility model should cover excursions of temperature and pH. When the BNA solubility model is incorporated into fuel performance models, the possible chemical combinations of the soluble species with other materials in the primary heat transport system can be evaluated.

2. Research Objectives

The goal of this project is to develop a thermodynamic treatment of the solubility of dysprosium and gadolinium sesquioxide (M_2O_3)* in ACR-1000 BNA material. It is anticipated that this treatment will permit the integration of this knowledge into future fuel performance codes involving existing computational means, or those currently under development by Piro, Lewis, and Thompson [5]. These extensive computations, nevertheless amenable to desktop computing, may involve many chemical elements in contact with the coolant solutions at varying pH and temperature. These are increasingly viewed as the backbone of future nuclear fuel development, such as that for the ACR-1000. In the present project, limited experimental work was undertaken to verify such matters as solubility products and solubility in alkaline media, as affected by complex ions of the form $Ln(OH)_n^{3-n}$ where Ln collectively refers to any of the chemically similar lanthanides. It is the expectation that the solubility treatment will be useful as a framework for such additional work (at coolant temperatures), as may be necessary in support of safety and licensing of the ACR-1000 reactor.

3. Solubility of BNA Pure Component Oxides

When anhydrous $Dy_2O_{3\,s}$ and other chemically similar lanthanide sesquioxides are introduced into water, it is commonly believed that a hydration reaction occurs (at least on the surface of the oxide particles) as shown below

$$Dy_2O_{3s} + 3H_2O = Dy_2O_3(H_2O)_{3s} \equiv 2Dy(OH)_{3s} \tag{1}$$

Note that the molar mass of the product for purposes of expressing the stoichiometry may either be regarded as a trihydrate or as an equivalent trihydroxide. The maximum concentration of dysprosium ion that eventually accumulates in the solution is thus determined by the chemical equilibrium below.

$$Dy(OH)_{3s} \rightarrow Dy_{aq}^{3+} + 3OH_{aq}^{-} \tag{2}$$

The foregoing process may equivalently be expressed as

$$Dy(OH)_{3s} + 3H_{aq}^{+} \rightarrow Dy_{aq}^{3+} + 3H_2O_l \tag{3}$$

In either case, an increase in acidity by raising the H^+ concentration or by lowering the OH^- concentration increases the Dy^{3+} concentration and thereby promotes the dissolution of $Dy(OH)_{3\,s}$. Dysprosium +3 aqueous ions are understood to be solvated by several water molecules. When dissolved in solutions of high alkalinity (pH>10), negative hydroxyl ions have a tendency to acquire a hydrogen atom from the surrounding water molecules to give rise to distinct chemical entities of the type $Dy(OH)_n^{(3-n)}$. This matter has a bearing on

* Sesquioxide is the general term for compounds containing 3 moles of oxygen and 2 moles of another element denoted by *M*.

$Dy(OH)_{3\ s}$ solubility. The concentration of Dy^{3+} is lowered thereby causing a shift to the right in the equilibria shown in equations (2) and (3). There is also the possibility that more than one hydroxyl ion (OH^-) may combine with Dy^{3+}_{aq} to form a series of species particularly as the alkalinity is raised to pH 14 or above. Speculated complexes are listed in Table .

Table 1. Aqueous species of dysprosium.

#	Various Aqueous Hydroxide Complexes of Dy Ions
1	Dy^{3+}_{aq}
2	$Dy(OH)^{2+}_{aq}$
3	$Dy(OH)^{+}_{2\ aq}$
4	$Dy(OH)_{3\ aq}$
5	$Dy(OH)^{-}_{4\ aq}$

It is likely that no more than four hydroxyl ions would arrange around the Dy^{3+}_{aq} ion because of steric-effects. Complexes of $Dy(OH)^{-}_{4\ aq}$ have been proposed by Haas *et al* [6].

Positive Complex Ion

In acidic solutions, the $Dy(OH)_{3\ s}$ consumes hydrogen ions (H^+) in the process of dissolution as indicated for example in Equation (4).

$$Dy(OH)_{3s} + 2H^{+}_{aq} \leftrightarrow \quad Dy(OH)^{2+}_{aq} \quad + \quad 2H_2O \qquad (4)$$

Here it is evident that as the pH decreases (H^+ concentration increases), there is an increase in the concentration of $Dy(OH)^{2+}_{aq}$ contributing to greater solubility of $Dy(OH)_{3\ s}$. The same line of reasoning would also apply to $Dy(OH)^{+}_{2\ aq}$.

Neutral Complex Ion

The formation of a neutral aqueous species, $Dy(OH)_{3\ aq}$, akin to the recognized neutral aqueous species *Li(OH),* would not affect the pH since H^+ or OH^- ions are not involved in the process of solubility.

$$Dy(OH)_{3s} \leftrightarrow \quad Dy(OH)_{3aq} \tag{5}$$

Negative Complex Ion

The formation of negative complex ions requires that $Dy(OH)_{3\,s}$ consume hydroxyl ions in the process of dissolution. Therefore, high alkalinity would favour increased solubility, the opposite of conventional expectations if $Dy(OH)^{-}_{4\,aq}$ were not recognized.

$$Dy(OH)_{3s} + OH^{-}_{aq} \leftrightarrow \quad Dy(OH)^{-}_{4aq} \tag{6}$$

The K_{sp} for equation (2) can be determined from a knowledge of the concentration of dysprosium and hydroxide ions in solutions of sufficient acidity to preclude high concentrations of the hydroxyl complex ions shown in Table . The solubility product can then be linked to the Gibbs energy by

$$\Delta G^{\circ}_{298K} = -RT\ \ln(K_{sp}) \tag{7}$$

The connection between the solubility and thermodynamic functions is made in this well-known expression only if Dy^{3+} is the predominant Dy-containing aqueous species. If hydroxyl complex ions of dysprosium truly exist at significant concentrations, then additional equilibria involving these ions are necessary to make possible the computation of the collective concentration of all dissolved dysprosium species coexisting with $Dy(OH)_{3\,s}$.

4. Experimental Work Supporting a Thermodynamic Treatment

The experimental work to provide thermodynamic property estimates of the various phases and species was divided into three categories:

1) Neutralization experiments to affirm the solubility products for $Dy(OH)_{3\,s}$ and $Gd(OH)_{3\,s}$.

2) Thermogravimetric analysis of the decomposition of the hydroxides and hydrates of Dy_2O_3 and Gd_2O_3 .

3) Neutron Activation Analytical analysis of saturated alkaline solutions ranging in pH from approximately 10 to 14.

5. Thermodynamic Modelling

The exploitation of a thermodynamic understanding of solubility is made possible though Gibbs energy minimization, an application of the Second Law of Thermodynamics. This powerful mathematical technique allows the consideration of a many coexisting equilibria potentially involving many phases. The integration of this procedure is just now becoming involved in nuclear fuel performance codes to capture the complex chemistry involved with large numbers of elements associated with nuclear fission by-products, and their potential exposure to coolant, fuel sheathing, and materials of reactor construction.

To enable, in a practical sense, the task of Gibbs energy minimization, computational software must be employed [7] requiring that the thermodynamic data of a all species be expressed in terms of Gibbs energy resulting from a knowledge (or estimate) of the enthalpy of formation from the elements (ΔH^o_T), the absolute entropy (S^o_T), and the heat capacity (C_p). The Gibbs energy at any temperature may be expressed by the following

$$G^\circ_T = \Delta H^\circ_T - T(S^\circ_T) \tag{8}$$

This Gibbs energy is sometimes called the "absolute" Gibbs energy in reference to the inclusion of the absolute entropy in the expression (instead of the entropy of formation from the elements). In truth, the Gibbs energy is a relative term that cannot be known absolutely; but, this expression is useful as a starting point in making comparisons of differences in the Gibbs energy between the various possible ways elements can be distributed among phases in varying concentrations.

The enthalpy and entropy terms in equation (8) can be expressed at various temperatures by integrating the heat capacity as shown below in Equations (9) and (10), respectively.

$$\Delta H^\circ{}_T = \Delta H^\circ{}_{298K} + \int_{298K}^{T} C_p \, dT \tag{9}$$

$$S^\circ{}_T = S^\circ{}_{298K} + \int_{298K}^{T} \frac{C_p}{T} \, dT \tag{10}$$

Combining Equations (9) and (10) into Equation (8)

$$G^\circ_T = \left[\Delta H^o_{298K} + \int_{298K}^{T} C_p \, dT \right] - T \left[S^o_{298K} + \int_{298K}^{T} \frac{C_p}{T} \, dT \right] \tag{11}$$

The thermodynamic data related to the hydroxide, monohydrate and complex ions species of dysprosium have been inferred through the preliminary solubility experimentation previously mentioned. These are shown in Table 2.

Table 2. Thermodynamic property dysprosium species.

Species	Phase	ΔH^{o}_{298K} (kJ·mol^{-1})	S^{o}_{298K} (J·mol^{-1}·K^{-1})	C_p (J·mol^{-1})
Dy	Solid	0	74.9	28.1
$Dy(OH)_3$	Solid	*-1409.2*	130.3	*115.0*
DyO(OH)	Solid	*-1084.0*	*120.0*	*100.0*
Dy_2O_3	Solid	-1863.1	149.8	115.4
Dy^{3+}	Aqueous	-698.7	-231.0	20.9
OH^-	Aqueous	-230.0	-10.9	-122.6
$Dy(OH)^{2+}_{aq}$	Aqueous	*-920.0*	*-130.0*	*0*
$Dy(OH)_2^{+}{}_{aq}$	Aqueous	*-1150.0*	*-30.0*	*0*
$Dy(OH)_{3\,aq}$	Aqueous	*-1395.0*	*70.0*	*0*
$Dy(OH)_4^{-}{}_{aq}$	Aqueous	*-1590.0*	*170.0*	*0*

*Estimate values in italics**.***

The estimated thermodynamic data for the representation of complexion foration is shown to follow a systematic linear trend. This was related to the increase in hydroxyl group additions of the form $Dy(OH)_n^{3-n}$, show in Figure 2 below.

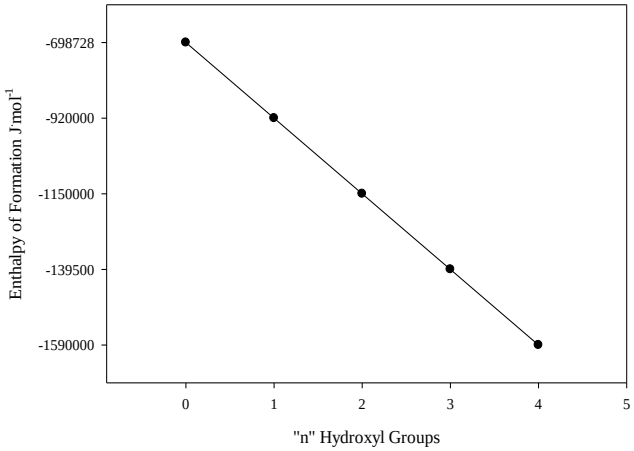

Figure 2. Linear enthalpy trends for final estimations made for dysprosium complex ions.

Solubility Model for Gadolinia

The processes for establishing estimates of complex ions and compounds of gadolinium were performed in accordance with the comparable treatment for dysprosium. Shown below in Table are the estimated thermodynamic properties for gadolinium species.

Table 5. Thermodynamic data for gadolinium species.

Component	Phase	ΔH^o_{298K} (kJ·mol^{-1})	S^o_{298K} (J·K^{-1}·mol^{-1})	C_p (J·K^{-1}·mol^{-1})
$GdO(OH)_s$	Solid	-1066.0	*120.0*	*100.0*
$Gd_2O_{3\,s}$	Solid	-1819.6	156.9	106.6
$Gd(OH)_{3s}$	Solid	*-1396.0*	*126.6*	*91.1*
Gd^{3+}_{aq}	Aqueous	-684.5	-205.853	-19.674
$Gd(OH)^{2+}_{aq}$	Aqueous	*-905.8*	*-105.0*	*0*
$Gd(OH)_2^{+}{}_{aq}$	Aqueous	*-1127.0*	*-5.0*	*0*
$Gd(OH)_{3\,aq}$	Aqueous	*-1348.3*	*95.0*	*0*
$Gd(OH)_4^{-}{}_{aq}$	Aqueous	*-1569.6*	*195.0*	*0*

*Estimate values in italics.

6. Computed Pourbaix Diagrams

A useful depiction of Gibbs energy minimization computations applied to aqueous systems is the stability diagram popularized by Pourbaix in his pioneering publication (*Atlas of Electrochemical Equilibria in Aqueous Solutions* [8]). These diagrams are isothermal plots generally at 25ºC indicating domains of stability of a particular chemical species on $E_h(V)$-pH coordinates. A review of Pourbaix diagram construction involving Gibbs energy minimization and the concepts discussed above is summarized in the Uhlig Corrosion Handbook [9], along with present work amplifying these diagrams to cover temperatures above 25ºC (in the next edition currently in press [10]).

Computed Pourbaix diagrams at 298 K for dysprosium, gadolinium and zirconium are shown on the left side of Figures 3 and 5 respectfully. These computed diagrams have been constructed to show the regions of aqueous stability for these proposed complex ions.

Since CANDU reactor coolant is maintained at elevated pressures and temperatures computed Pourbiax diagrams have been projected to temperatures of 550 K (left of Figures 3 and 5), closer to actual operation. It is of note that in Figures 3 and 4 for dysprosium and gadolinium, respectively, the regions of stability for the complex ions becomes larger than that at conditions of 298 K. This is reflective of the fact that an increase in temperature also increases the solubility of the BNA. However, regardless of the temperature conditions shown, the solubility still maintains a negligible concentration, in solution validating the previous belief that if the coolant can into contact with the BNA material that that the concentration leached would not pose a safety concern with affecting the neutron economy of the reactor.

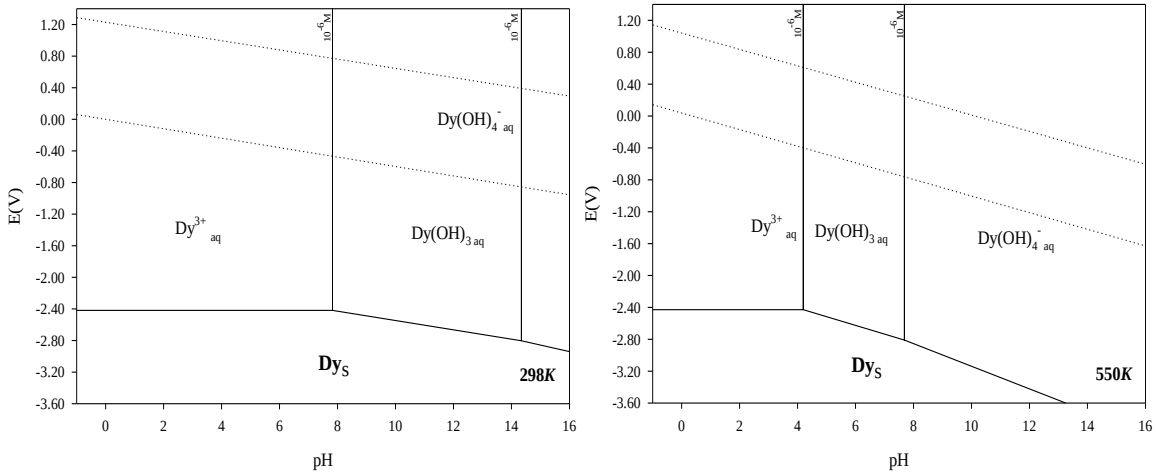

Figure 3. The Pourbaix diagram for dysprosium at 298 K (left) and 550 K (right) for an aqueous concentration of 10^{-6} molal.

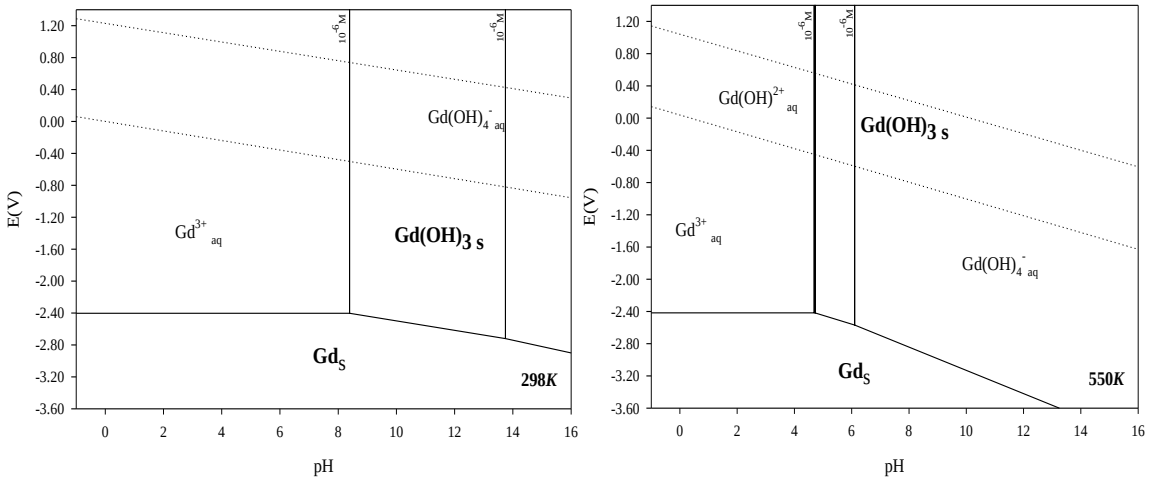

Figure 4. The Pourbaix diagram for gadolinium at 298 K (left) and 550 K (right) for an aqueous concentration of 10^{-6} molal.

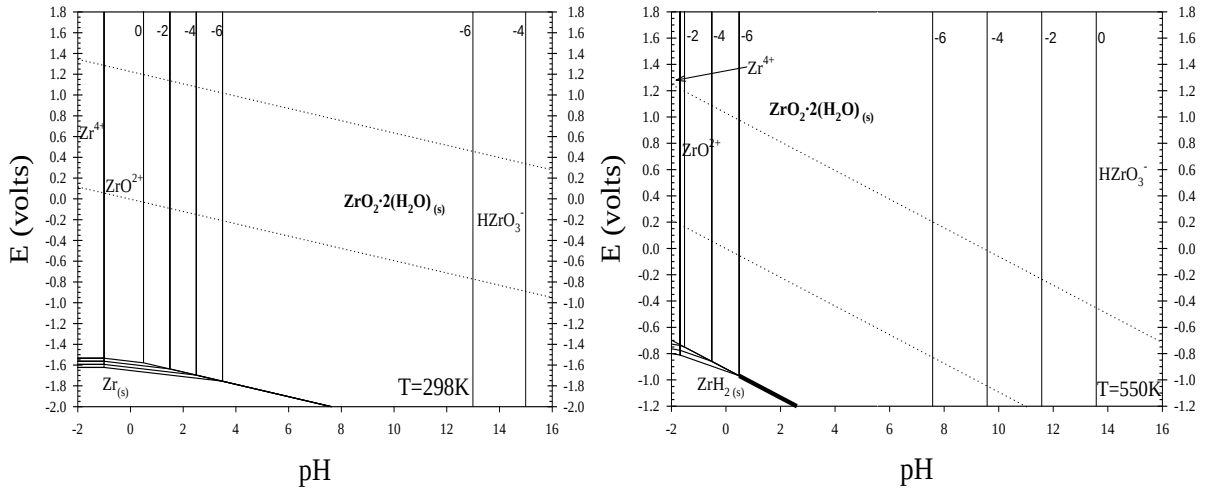

Figure 5. The Pourbaix diagram for zirconium at 298 K (left) and 550 K (right) for an aqueous concentration 1, 10^{-2}, 10^{-4}, and 10^{-6} molal [10].

7. Solubility Computation of BNA at Elevated Temperatures

There are many considerations in computing the solubility in a multi-component system involving many possible species and phases, not to mention the concerns involved in achieving equilibrium. Herein lies the necessity of a powerful computational technique such as Gibbs energy minimization, to which the solubility framework in the present thesis is addressed.

Let us consider, for example, water containing a small number of moles of BNA with an arbitrary composition (mol fractions of and are both 0.1). The water phase is understood to be made alkaline with a low concentration of lithium hydroxide. This is further made reducing by the small addition of dissolved hydrogen gas (representative of reactor coolant). This is to be understood as a simplified system for the discussion of BNA solubility.

To visualize the computation proposed, refer to Figure 6 for 550 K. The coolant, made alkaline with lithium hydroxide, is shown in light blue. Represented below the coolant is a section of hypothetical BNA pellet surface (light gray) that would come into contact with the coolant if there were a sheath breach in the central element of the ACR-1000 fuel bundle. The final equilibrium condition is shown below the downward pointing bold arrow; this is the computed equilibrium using Gibbs energy minimization.

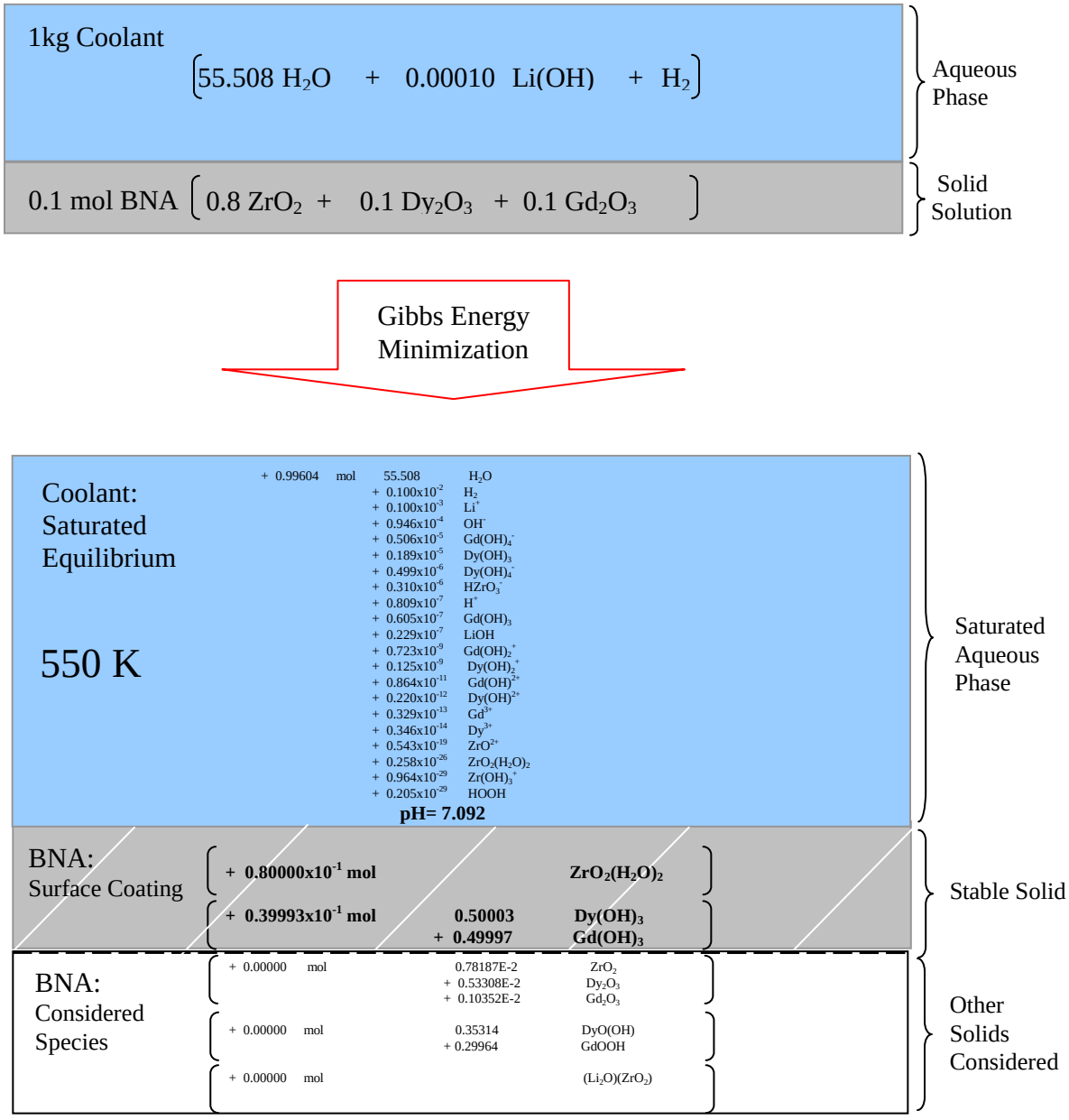

Figure 6. Solubility computation of an arbitrarily chosen BNA composition at 550 K.

Once equilibrium is reached, represented by the state after Gibbs energy minimization, the coolant is shown to become saturated with the proposed aqueous species of dissolved BNA material. Equilibrium computations have also indicated that aqueous species of dysprosium and gadolinium become more soluble and therefore more dominant in the aqueous phase than species of zirconium. The extent to which these species of dysprosium and gadolinium leach into the saturated coolant is limited. As previously mentioned, once these oxides are in contact with water, they form a surface coating of each respective hydroxide or in the case of zirconia, a dihydrate (above the dashed line representing the surface coating). It is these two solid phases

($ZrO_{2\,s}(H_2O)_{2s}$, and { $(Dy,Gd)(OH)_{3s}$ }) which are considered to be controlling the solubility. In this treatment, the chemically similar and are considered to form an ideal solid solution (denoted by {}), making the activity of each component hydroxide equal to the mole fraction.

A limitation on the dissolution of Dy and Gd may be attributed to the fact that the coolant is saturated with zirconium. Once the hydroxides of dysprosium and gadolinium on the thin surface coating leach, it would become progressively more difficult for Dy and Gd some distance under the pellet surface to dissolve, since solid state diffusion is required. It is thought that further significant dissolution would be hindered by the general saturation of coolant with zirconium dihydrate (covering all Zircaloy through which the coolant must pass). In performing the Gibbs energy minimization computations, other solid species and solid solutions were considered. These are shown below the dashed line. However, the inclusion of these possible phases in the equilibrium assemblage does not contribute to lowering the Gibbs energy of the system and these compounds show zero mols formed.

Figure 6 is suggestive of how the current solubility treatment could be useful in not only modelling effects of temperature and pressure, but also on how to plan high temperature experimentation in order to yield data to improve the current model. In particular, these figures draw attention to the difficulty of sampling hot saturated solutions that may precipitate before chemical analysis can be performed.

8. Conclusions

A framework to model solubility with thermodynamic parameters for the various aqueous species and phases has been proposed. Solubility measurements were conducted on dysprosium oxide ($Dy_2O_{3\,s}$) and gadolinium oxide ($Gd_2O_{3\,s}$) at room temperature and pressure conditions, yielding the solubility products of each trihydroxide. Thermogravimetric analysis provided the decomposition behaviour of the hydroxides as well as the monohydrates. It was concluded that the solubility of $Dy_2O_{3\,s}$ and $Gd_2O_{3\,s}$ (collectively $Ln_2O_{3\,s}$) is controlled by a superficial formation of trihydroxide ($Ln(OH)_{3\,s}$ or equivalently trihydrate ($Ln_2O_3 \cdot 3H_2O_s$).Solubility measurements and related thermodynamic information were interpreted and expressed on the supposition that complex ions of the type $Ln(OH)_n^{3-n}$ exist (n=1 to 4). Estimates of the entropy of proposed complex ions and other aqueous species were established in order that Gibbs energy minimization calculations could be made at elevated temperatures associated with conditions in a reactor. Pourbaix diagrams were calculated for Dy and Gd at 298 K and 550 K using the proposed thermodynamic properties and other accepted data to establish domains of stability in redox potential - pH space. It is generally concluded that the low solubility of dysprosium and gadolinium in coolant with pH near 10 (measured at 298 K) does not pose a safety concern with respect to the issue of neutron economy in ACR-1000 operation caused by a defected central element. The usefulness of this framework is due to the versatility in which it can be applied. Modelling the solubility of BNA materials in this fashion allows for its easy incorporation into other fuel performance codes, particularly in the projects currently undertaken in the Nuclear Fuel group at RMC.

9. References

1. Atomic Energy of Canada Limited, "ACR-1000 Technical Summary: An Evolution of CANDU®", Atomic Energy of Canada Limited (2007).
2. D. Torgerson, "The ACR-700 – Raising The Bar for Reactor Safety Performance, Economics and Constructability", Nuclear News 45 (2002) 24-32.
3. P. Boczar, "Advanced Fuel Development in AECL", Canadian Nuclear Society Bulletin 24 (2005) 17-24.
4. G. Erdtmann, "Neutron Activation Tables", 6th Ed., Kerchemie in Einzeldarstellungen, Verlag Chemie, New York, United States (1976).
5. M. Piro, M. Welland, B. Lewis, and W. Thompson, "Development of a Self Standing Numerical Tool to Compute Chemical Equilibria in Nuclear Materials", Proceedings of Top Fuel Conference, Paris, France (2009).
6. J. Haas, E. Shock, and D. Sassani, "Rare Earth Elements in Hydrothermal Systems: Estimates of Standard Partial Molal Thermodynamic Properties of Aqueous Complexes or the Rare Earth Elements at High Pressure and Temperatures", Geochemica et Cosmochimica Acta 59 21 (1995) 4329-4350.
7. C. Bale, A. Pelton, and W. Thompson, "Facility for the Analysis of Chemical Thermodynamics", Ecole Polytechnique, Montréal, Canada (2002).
8 . M. Pourbaix, "Atlas of Electrochemical Equilibria in Aqueous Solutions", Pergamon Press Ltd. Bristol, England (1966).
9. W. Thompson, M. Kaye, C. Bale, and A. Pelton, "Pourbaix Diagrams for Multielement Systems", Uhlig's Corrosion Handbook 2nd Ed., Ed. R. Winston Reveie, John Wiley and Sons Incorporated, New York, United States (2000) 125-136.
10. M. Kaye, and W. Thompson, "Computation of Pourbaix Diagrams at Elevated Temperatures", Royal Military College, Kingston, Ontario, Canada, (2009).